A printed nanobeam laser on a SiO_2/Si substrate for low-threshold continuous-wave operation

Indra Karnadi,[1,5] Jaehyeon Son,[2,5] Ju-Young Kim,[2] Hoon Jang,[1] Seungwoo Lee,[2,3] Ki Soo Kim,[4] Bumki Min,[2,6] and Yong-Hee Lee[1,*]

[1] *Department of Physics, Korea Advanced Institute of Science and Technology (KAIST), Daejeon 305-701, South Korea*

[2] *Department of Mechanical Engineering, Korea Advanced Institute of Science and Technology (KAIST), Daejeon 305-701, South Korea*

[3] *SKKU Advanced Institute of Nanotechnology (SAINT) & School of Chemical Engineering, Sungkyunkwan University (SKKU), Suwon440-746, South Korea*

[4] *Convergence and Components& Materials Research Laboratory, Electronics and Telecommunications Research Institute, Daejeon 305-700, South Korea*

[5] *These authors contributed equally.*

[6] *bmin@kaist.ac.kr*

[*] *yhlee@kaist.ac.kr*

Abstract: A small-footprint nanobeam photonic crystal laser made of InGaAsP material is directly integrated on a SiO_2/Si substrate without using adhesive material via transfer-printing processes (i.e., dry transfer-printing). The transferred nanobeam structure with a physical volume of ~6.6 × 0.58 × 0.28 μm^3 (~10.5 $(\lambda/n)^3$) shows single mode lasing near 1550 nm with continuous-wave (CW) operation at room-temperature, where effective lasing threshold power was as low as 9 μW. This CW operation was achieved mainly due to efficient heat dissipation provided by direct contact between the nanobeam and the substrate. This transfer-printed nanobeam laser could be a promising candidate for the next-generation light source with a feature of low-power consumption in ultracompact photonic integrated circuits.

©2014 Optical Society of America

OCIS codes: (140.0140) Lasers and laser optics; (160.5298) Photonic crystals; (250.5960) Semiconductor lasers.

References and links

1. G. Roelkens, J. Van Campenhout, J. Brouckaert, D. Van Thourhout, R. Baets, P. Rojo Romeo, P. Regreny, A. Kazmierczak, C. Seassal, X. Letartre, G. Hollinger, J. M. Fedeli, L. D. Cioccio, and C. L. Blanchard, “III-V/Si photonics by die-to-wafer bonding,” Mater. Today **10**(7–8), 36–43 (2007).
2. G. Roelkens, L. Liu, D. Liang, R. Jones, A. Fang, B. Koch, and J. Bowers, “III-V/silicon photonics for on-chip and inter-chip optical interconnects,” Laser Photon. Rev. **4**(6), 751–779 (2010).
3. D. Liang and J. E. Bowers, “Recent progress in lasers on silicon,” Nat. Photonics **4**(8), 511–517 (2010).
4. H. Yang, D. Zhao, S. Chuwongin, J.-H. Seo, W. Yang, Y. Shuai, J. Berggren, M. Hammar, Z. Ma, and W. Zhou, “Transfer-printed stacked nanomembrane lasers on silicon,” Nat. Photonics **6**(9), 615–620 (2012).
5. Y. Zhang, M. Khan, Y. Huang, J. Ryou, P. Deotare, R. Dupuis, and M. Lončar, “Photonic crystal nanobeam lasers,” Appl. Phys. Lett. **97**(5), 051104 (2010).
6. Y. Gong, B. Ellis, G. Shambat, T. Sarmiento, J. S. Harris, and J. Vuckovic, “Nanobeam photonic crystal cavity quantum dot laser,” Opt. Express **18**(9), 8781–8789 (2010).
7. B. Ellis, M. A. Mayer, G. Shambat, T. Sarmiento, J. Harris, E. E. Haller, and J. Vuckovic, “Ultralow-threshold electrically pumped quantum-dot photonic-crystal nanocavity laser,” Nat. Photonics **5**(5), 297–300 (2011).
8. K.-Y. Jeong, Y.-S. No, Y. Hwang, K.-S. Kim, M.-K. Seo, H.-G. Park, and Y.-H. Lee, “Electrically driven nanobeam laser,” Nat. Commun. **4**, 2822 (2013).
9. K. Nozaki, S. Kita, and T. Baba, “Room temperature continuous wave operation and controlled spontaneous emission in ultrasmall photonic crystal nanolaser,” Opt. Express **15**(12), 7506–7514 (2007).
10. J. Huang, S.-H. Kim, J. Gardner, P. Regreny, C. Seassal, P. A. Postigo, and A. Scherer, “Room temperature, continuous-wave coupled cavity InAsP/InP photonic crystal laser with enhanced far-field emission directionality,” Appl. Phys. Lett. **99**(9), 091110 (2011).

11. S. Matsuo, K. Takeda, T. Sato, M. Notomi, A. Shinya, K. Nozaki, H. Taniyama, K. Hasebe, and T. Kakitsuka, "Room-temperature continuous-wave operation of lateral current injection wavelength-scale embedded active-region photonic-crystal laser," Opt. Express **20**(4), 3773–3780 (2012).
12. M. H. Shih, A. Mock, M. Bagheri, N.-K. Suh, S. Farrell, S.-J. Choi, J. D. O'Brien, and P. D. Dapkus, "Photonic crystal lasers in InGaAsP on SiO_2/Si substrate and its thermal impedance," Opt. Express **15**(1), 227–232 (2007).
13. G. Vecchi, F. Raineri, I. Sagnes, A. Yacomotti, P. Monnier, T. J. Karle, K.-H. Lee, R. Braive, L. Le Gratiet, S. Guilet, G. Beaudoin, A. Taneau, S. Bouchoule, A. Levenson, and R. Raj, "Continuous-wave operation of photonic band-edge laser near 1.55 µm on silicon wafer," Opt. Express **15**(12), 7551–7556 (2007).
14. L. J. Martínez, B. Alén, I. Prieto, J. F. Galisteo-López, M. Galli, L. C. Andreani, C. Seassal, P. Viktorovitch, and P. A. Postigo, "Two-dimensional surface emitting photonic crystal laser with hybrid triangular-graphite structure," Opt. Express **17**(17), 15043–15051 (2009).
15. Y. Halioua, A. Bazin, P. Monnier, T. J. Karle, I. Sagnes, G. Roelkens, D. Van Thourhout, F. Raineri, and R. Raj, "III-V photonic crystal wire cavity laser on silicon wafer," J. Opt. Soc. Am. B **27**(10), 2146–2150 (2010).
16. Y. Halioua, A. Bazin, P. Monnier, T. J. Karle, G. Roelkens, I. Sagnes, R. Raj, and F. Raineri, "Hybrid III-V semiconductor/silicon nanolaser," Opt. Express **19**(10), 9221–9231 (2011).
17. T.-W. Lu, W.-C. Tsai, T.-Y. Wu, and P.-T. Lee, "Laser emissions from one-dimensional photonic crystal rings on silicon-dioxide," Appl. Phys. Lett. **102**(5), 051103 (2013).
18. W. S. Fegadolli, S.-H. Kim, P. A. Postigo, and A. Scherer, "Hybrid single quantum well InP/Si nanobeam lasers for silicon photonics," Opt. Lett. **38**(22), 4656–4658 (2013).
19. M. A. Meitl, Z.-T. Zhu, V. Kumar, K. J. Lee, X. Feng, Y. Y. Huang, I. Adesida, R. G. Nuzzo, and J. A. Rogers, "Transfer printing by kinetic control of adhesion to an elastomeric stamp," Nat. Mater. **5**(1), 33–38 (2006).
20. B. Wang, T. Siahaan, M. A. Dundar, R. Notzel, S. He, and R. W. van der Heijden, "Transfer printing and nanomanipulating luminescent photonic crystal membrane nanocavities," J. Appl. Phys. **111**(9), 093105 (2012).
21. M. Notomi, E. Kuramochi, and H. Taniyama, "Ultrahigh-Q nanocavity with 1D photonic gap," Opt. Express **16**(15), 11095–11102 (2008).
22. P. B. Deotare, M. W. McCutcheon, I. W. Frank, M. Khan, and M. Lončar, "High quality factor photonic crystal nanobeam cavities," Appl. Phys. Lett. **94**(12), 121106 (2009).
23. B.-S. Song, S. Noda, T. Asano, and Y. Akahane, "Ultra-high-Q photonic double-heterostructure nanocavity," Nat. Mater. **4**(3), 207–210 (2005).
24. H.-G. Park, J.-K. Hwang, J. Huh, H.-Y. Ryu, S.-H. Kim, J.-S. Kim, and Y.-H. Lee, "Characteristics of modified single-defect two-dimensional photonic crystal lasers," IEEE J. Quantum Electron. **38**(10), 1353–1365 (2002).
25. M. Shearn, X. Sun, M. D. Henry, A. Yariv, and A. Scherer, "Advanced plasma processing: etching, deposition, and wafer bonding techniques for semiconductor applications," in *Semiconductor Technologies*, J. Grym, ed. (InTech, 2010), pp. 80–104.
26. K. Nozaki, A. Nakagawa, D. Sano, and T. Baba, "Ultralow threshold and single-mode lasing in microgear lasers and its fusion with quasi-periodic photonic crystals," IEEE J. Sel. Top. Quantum Electron. **9**(5), 1355–1360 (2003).
27. H.-Y. Ryu, H.-G. Park, and Y.-H. Lee, "Two-dimensional photonic crystal semiconductor lasers: computational design, fabrication, and characterization," IEEE J. Sel. Top. Quantum Electron. **8**(4), 891–908 (2000).
28. T. Baba, "Photonic crystals and microdisk cavities based on GaInAsP-InP system," IEEE J. Sel. Top. Quantum Electron. **3**(3), 808–830 (1997).
29. S.-L. Chuang, *Physics of Photonic Devices* (Wiley, 2009).

1. Introduction

Having been employed to implement a reliable light source in various optical devices over the past few decades, III-V semiconductors are now proven to be a versatile platform for industrial applications such as VCSEL telecommunications or optical interconnects. Combining them with silicon (Si) photonics that inherit the maturity of complementary metal–oxide–semiconductor (CMOS) processing technologies, one could pave the way for realizing low-cost next-generation photonic integrated circuits (PICs) [1–4]. In addition to the possibility of low-cost production, the future PIC should also exhibit other important properties such as ultracompact size and low power consumption, which are essential for making high density on-chip photonic networks with low energy cost. Therefore, a small footprint and low threshold light source made of III-V semiconductors needs to be integrated on a silicon chip. Moreover, in order to diversify the functionalities of the device, CW operation of the light source is also highly desired. To accommodate all these requirements, photonic crystal (PC) laser has been widely studied as a promising candidate because of its remarkable properties such as compact-size and low-threshold [5–8], and its ability to operate as a CW laser [9–11].

Indeed, there have recently been several efforts to integrate III-V quantum well (QW) PC lasers on Si-chips [12–18]; various wafer bonding techniques such as molecular bonding [12,14,18], adhesive bonding [15–17], and metallic dry bonding [13] have been proposed and employed to bond the III-V QW material onto Si substrate prior to the fabrication of PC laser structures. Among these techniques, the adhesive bonding method is most widely used due to the fact that it does not have stringent interface requirements in contrast to the other bonding processes. However, the presence of adhesive material that typically has poor thermal conductivity hinders heat transfer from the PC laser to the substrate, which makes room temperature CW operation of PC lasers more difficult to achieve.

The CW operation of III-V QWs PC laser on a Si substrate at room temperature was first reported by Vecchi et al [13] using 2D band-edge honeycomb lattice configuration. In this case, the InGaAs/InP material is bonded onto the Si substrate by using metallic dry bonding method with SiO_2 as a cladding layer. The use of SiO_2 and metal as a cladding layer and the bonding agent, respectively, give efficient thermal dissipation through the substrate, which enables the CW operation of PC laser. While they have shown the feasibility of CW lasing in the bonded structure, the 2D scheme of PC structure leads to relatively large device footprint as the lateral dimension of the device is often larger than ~30 × 30 μm^2. In addition, the geometry of the honeycomb lattice restricts the integration with an external coupler. Therefore, a careful consideration is further required to overcome these limitations for a reliable light source in PIC.

In this work, we demonstrate an integration of a small-footprint InGaAsP nanobeam laser on a SiO_2/Si substrate without using any adhesive material via transfer-printing process (i.e., dry transfer-printing) [4, 19, 20], where direct contact with the SiO_2/Si substrate provides efficient heat dissipation for the laser [13]. With a help of micron-sized polydimethylsiloxane (PDMS) stamp developed by soft-lithography (the ratio of curing agent to base was 0.1), the nanobeam was selectively released from its parent chip and directly printed on a foreign substrate (herein, SiO_2/Si substrate). By using this method, complex fabrication processes generally involved in the wafer bonding schemes could be significantly simplified. Besides, it is also efficient to reduce the consumption of InGaAsP material, because only small portion of it is patterned, retrieved, and printed on the receiver substrate. Here, we choose the nanobeam as the PC platform because it has some unique features such as simple architecture, small footprint, high-Q factor, and small mode volume [5, 6, 8, 21, 22]. Furthermore, the 1D nature of the nanobeam leads to a straightforward integration with an external coupler. The printed nanobeam has 16 air-holes and occupies physical volume of ~6.6 × 0.58 × 0.28 μm^3. With this structural design, we observed single mode lasing near 1550 nm with CW operation at room temperature. To the best of our knowledge, this is the first demonstration of room temperature CW operation of printed nanobeam laser working near 1550 nm.

2. Nanobeam design

The nanobeam structure is composed of an InGaAsP ridge-waveguide with thickness (t) of 280 nm and width (w) of 580 nm (Fig. 1(a)). Along the waveguide, periodic air-holes with a lattice constant of 430 nm are introduced except for a central photonic well region. The photonic well, where photons with a specific frequency can be confined, is constructed by modulating the cutoff frequency of the dielectric band [21]. In order to generate resonant modes with less scattering losses, the Gaussian-like photonic well is introduced [23]. This kind of photonic well is very efficient in suppressing the Fourier components of the resonant mode in the radiation zone. As a result, the scattering losses into the substrate modes and free-space modes could be substantially reduced. In our design, the photonic well is formed by reducing the lattice constant of three air-holes towards the center of the waveguide linearly from 390 nm to 310 nm. The ratio of air hole radius (r) to lattice constant (a) in all regions is fixed at $r = 0.34a$. As shown in Fig. 1(b), the spatial distribution of the cutoff frequency follows the Gaussian shaped function. At the end of the nanobeam, two small breakable

#208787 - $15.00 USD Received 24 Mar 2014; revised 3 May 2014; accepted 4 May 2014; published 12 May 2014
(C) 2014 OSA

tethers with width of 100 nm and length of 430 nm were additionally introduced (see the geometry of the nanobeam in Fig. 1(b)). By introducing these two small tethers, the freestanding nanobeam can be released easily from its parent chip just by applying a small impulse force on top of it.

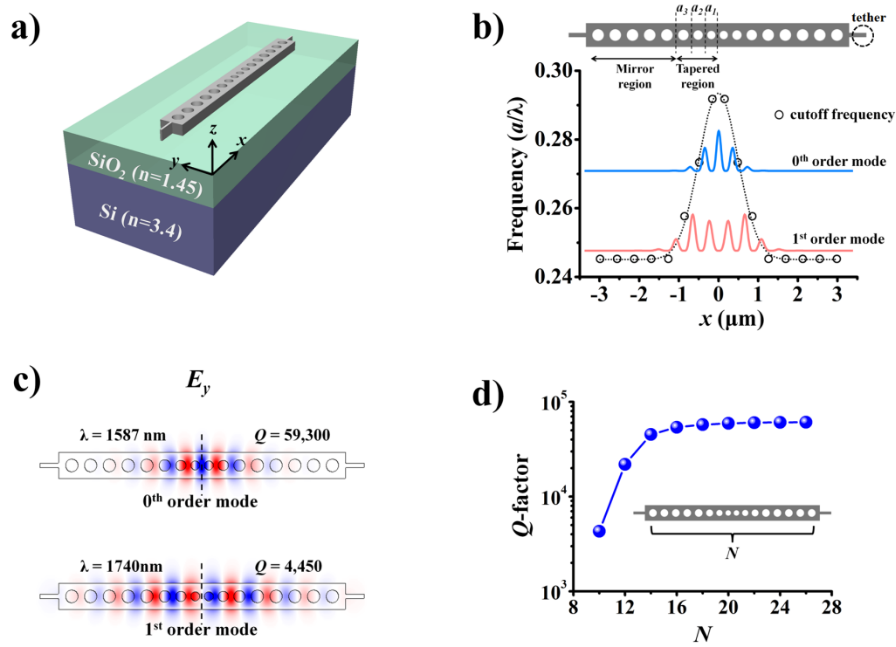

Fig. 1. (a) Schematic of nanobeam on a SiO_2/Si substrate. (b) Formation of a photonic well. (c) E_y field profile of 0th order and 1st order modes of the nanobeam in (a). (d) Q-factor of the nanobeam as a function of total number of air holes (N).

In order to identify the resonant modes of the structure, 3D-FDTD simulation were performed. In the simulation, the refractive indices of the PC slab, SiO_2, and Si are set to 3.4, 1.45 and 3.46, respectively. The buffer SiO_2 layer has thickness of 2 μm, which is thick enough to provide adequate optical isolation of the nanobeam from the Si substrate. Figure 1(c) shows the E_y field profiles of the 0th order and 1st order modes of the nanobeam on a SiO_2/Si substrate. The 0th order and 1st order mode have resonant wavelengths of 1587 nm and 1740 nm, respectively. The large free spectral range between these resonant modes is advantageous in exciting only a single mode within the gain bandwidth of the active medium. The Q-factor of the 0th order mode as a function of total number of air holes (N) is plotted in Fig. 1(d), where the Q-factor is found out to be saturated for $N \geq 16$. Thus, $N = 16$ was chosen for the fabrication with the consideration of device footprint and performance. The Q-factor and mode volume of the 0th order mode for $N = 16$ are 5.93×10^4 and $0.25(\lambda/n)^3$, respectively.

3. Fabrication process

Based on the above design, the nanobeam was fabricated on a 280-nm-thick InGaAsP slab that contained three QWs in the middle as an active medium. It was fabricated by following a series of standard nanofabrication processes [24]: e-beam lithography, Cl_2 assisted Ar-beam etching, O_2 ashing, and selective wet etching by using HCl solution (HCl:water = 4:1) at room temperature. Figure 2(a) shows SEM images of the fabricated nanobeam.

#208787 - $15.00 USD Received 24 Mar 2014; revised 3 May 2014; accepted 4 May 2014; published 12 May 2014
(C) 2014 OSA

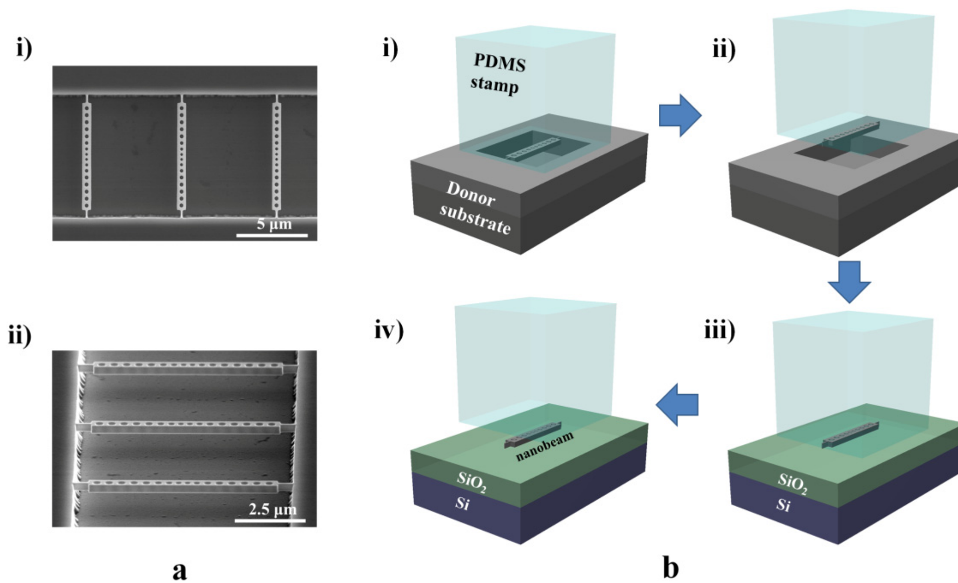

Fig. 2. (a) SEM images of the fabricated sample i) top and ii) tilted view. (b) Schematic of the transfer-printing processes i) micron-sized, rectangular PDMS stamp (15 µm × 15 µm × 40 µm) was precisely aligned and placed on the top of the nanobeam. A small impulse force was applied on the stamp in order to break two small tethers at the end of the nanobeam. ii) After breaking the tethers, the nanobeam will be attached to the stamp due to non-specific, general van der Walls force. iii) PDMS stamp inked with the nanobeam is put in contact with the receiver substrate. iv) The stamp is retracted slowly in order to separate it from nanobeam by kinetically controlled viscoelastic effect of PDMS.

The fabricated InGaAsP nanobeam was integrated on a SiO_2/Si substrate by means of transfer-printing processes. The processes are schematically illustrated in Fig. 2(b). First, the PDMS stamp with transverse dimensions of 15 µm × 15 µm and height of 40 µm was placed on the top of the nanobeam. In order to break two small tethers at the end of the nanobeam, a small impulsive load was applied on the stamp. Due to the non-specific, general van der Waals force, the nanobeam will be attached to the stamp even after the tethers are broken. The next process is the transfer of nanobeam onto the SiO_2/Si substrate. Before the transfer, the substrate was first cleaned in RCA-1 solution and then slightly treated by atmospheric oxygen plasma to generate a smooth and reactive thin oxide layer on its surface [25]. This thin oxide layer helps in enhancing the adhesion between the nanobeam and the substrate. After putting the nanobeam in contact with the receiver substrate, the PDMS stamp is retracted slowly (~10 µm/s) in order to separate it from the nanobeam. Especially, the intrinsic viscoelastic nature of the PDMS enables efficient adhesion switching in dry-adhesion merely by control of pulling speed of the stamp, so that the nanobeam with high structural fidelity can be directly printed onto a SiO_2/Si substrate without any adhesives [19]. Figure 3(a) shows SEM images of the integrated device; it is clearly seen that the nanobeam with high structural fidelity (without any deformations) is conformably printed onto a SiO_2/Si substrate.

4. Optical measurement

Laser emission from the nanobeam is characterized while vertically pumping the sample with a 980 nm InGaAs laser diode under CW operation at room temperature. A microscope objective lens (× 50) with NA of 0.85 is used to focus the pump beam to a spot ~3.2 µm diameter and to collect the emitted light from the sample at the same time. Figure 3(b) shows the photoluminescence (PL) spectrum acquired from the sample above the lasing threshold. From the spectrum, a single peak at 1589 nm corresponding to the 0th order mode is observed

without any other lasing modes over 100 nm wavelength range. In the insets of Fig. 3(b), the lasing-mode image captured by a charge-coupled device camera and the polarization dependence of the laser emission are shown. The emitted beam is dominantly *y*-polarized (perpendicular to the length of the nanobeam) with a polarization extinction ratio of 12:1. This polarization dependency indicates the transverse electric-like characteristic of the resonant mode.

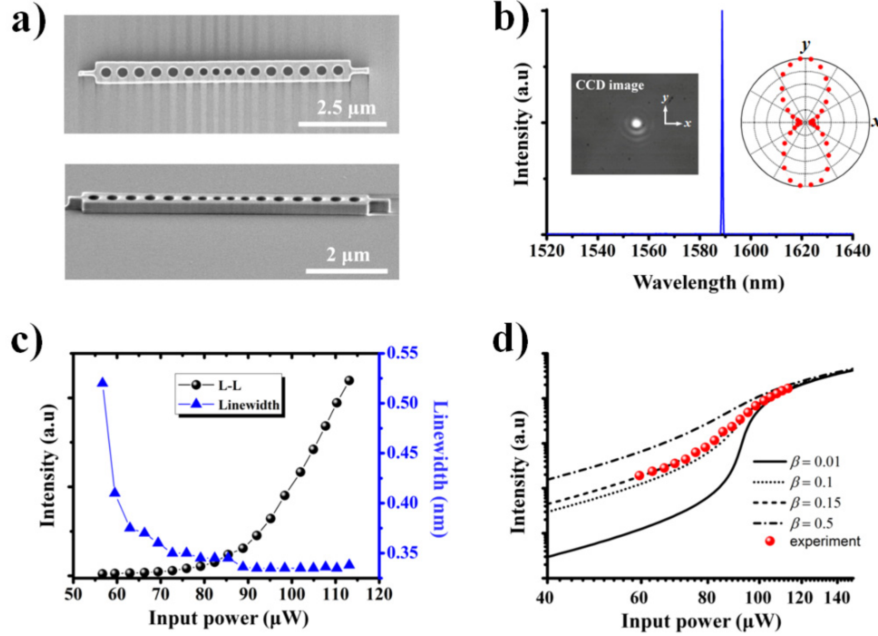

Fig. 3. (a) SEM images of the printed nanobeam on a SiO_2/Si substrate taken at top view (top panel) and side view (bottom panel): the nanobeam was conformably printed on a SiO_2/Si substrate. (b) Photoluminescence spectrum of the nanobeam printed on a SiO_2/Si substrate. Insets show the lasing-mode image captured by a CCD camera and the polarization dependence of the laser emission. (c) L-L curve and spectral linewidth as a function of input pump power of the 0thmode. (d) Rate equation fitted L-L measurement on log-log scales.

The light-out versus light-in (L-L) curve of the fabricated laser and its spectral linewidth as a function of input pump power are plotted in Fig. 3(c). The linewidth plot clearly shows the spectral narrowing from the spontaneous emission regime to the laser emission. It changes abruptly near the threshold and decreases to the resolution limit (~0.33 nm) of the spectrometer above the threshold. The lasing threshold is estimated to be ~90 µW in terms of the input pump power. By considering the overlapping area between the pumping spot and the nanobeam (23%) and the absorption efficiency of irradiated light in the slab (43%) [26], it can be estimated that only ~10% of the pump power is absorbed. This gives the effective threshold of ~9 µW. This low threshold is attributed to a small active volume of the nanobeam since the low input power is required to make a small active volume be transparent [8]. Another factor such as large Q/V also contributes to the low threshold of the nanobeam laser. The gradual change near the threshold in the L-L curve implies a large value of spontaneous emission factor (β) [27]. In order to estimate the β-factor of our fabricated sample, the experimental L-L curve is fitted using conventional laser rate equations [27–29]. In the equations, carrier density (N) and photon density (P) of the nanobeam laser are described as follow:

$$\frac{dN}{dt} = \eta \frac{L_{in}}{\hbar\omega_p V_a} - \left(\frac{A_a}{V_a} v_s N + BN^2 + CN^3\right) - \Gamma G(N)P \tag{1}$$

#208787 - $15.00 USD Received 24 Mar 2014; revised 3 May 2014; accepted 4 May 2014; published 12 May 2014
(C) 2014 OSA

$$\frac{dP}{dt} = \Gamma G(N)P - \frac{P}{\tau_p} + \beta BN^2 \tag{2}$$

Table 1. Parameters Used in the Rate Equations

Parameters	Values
Active surface area in the pumped active region (A_a)	0.26×10^{-8} cm^2
Active region volume in the pumped active region (V_a)	0.28×10^{-13} cm^3
Surface recombination velocity (v_s)	1.5×10^4 cm s^{-1}
Bimolecular recombination coefficient (B)	1.0×10^{-10} cm^3 s^{-1}
Auger non-radiative recombination rate (C)	5.0×10^{-29} cm^6 s^{-1}
Confinement factor (Γ)	0.075
Gain coefficient (G_0)	1500 cm^{-1}
Transparency current density (N_{tr})	1.0×10^{18} cm^{-3}
Q-factor (Q)	4300
Effective refractive index (n_{eff})	2.51
Lasing wavelength (λ_{out})	1589 nm
Pump laser wavelength (λ_p)	980 nm

The definitions of parameters and their value are listed in Table 1. Here, the logarithmic gain was assumed to be $G(N) = G_0c/n_{eff} \ln(N/N_{tr})$. The frequency of pump laser ω_p and photon lifetime τ_p are given by $\omega_p = 2\pi c/\lambda_p$ and by $\tau_p = \lambda_{out}Q/2\pi c$, respectively. The spontaneous emission factor, β, and the absorption ratio of the pump laser in the QWs, η, are set as variables in Eqs. (1) and (2). The output power $L_{out} = \hbar\omega_{out}PV_a/\tau_p$ is plotted as a function of input power L_{in}. Figure 3(d) shows the logaritmic plot of L-L curve calculated from the rate equation with different values of β. The best fitting is obtained when $\beta = 0.15$ and $\eta = 0.10$. This β value is mainly limited by the Q-factor, $Q = 4.3 \times 10^3$, that we used in the rate equations. In our case, the Q-factor is estimated from the full width at half maximum of the resonant peak near the transparency and is limited by the resolution of our spectrometer. The actual Q-factor and therefore β is expected to be larger than this value.

5. Summary

In summary, we have experimentally demonstrated the direct integration of the small footprint InGaAsP nanobeam laser on a SiO_2/Si substrate by means of dry transfer-printing technique. From the structure, room temperature CW operation near 1550 nm with effective threshold of ~9 μW was achieved. There are two criteria that need to be fulfilled in order to reach room temperature CW operation in PhC laser, i.e. low lasing threshold and better heat sink. The proposed structure of our nanobeam laser satisfies these two criteria; (i) the small active volume and large Q/V of the nanobeam results in low threshold input power, and (ii) the presence of a SiO_2/Si as a substrate provides advanced integration strategy for the device with a better heat dissipation. This heat dissipation could be further improved by optimizing the thickness of SiO_2 layer or encapsulating the top side of the device with low index material that has better thermal conductivity than air.

Acknowledgments

The work at Lee group (I.K., H.J. and Y.H.L.) was supported by National Research Foundation of Korea (NRF) grant funded by the Korea government (MEST) (NRF-2007-0093863), Basic Science Research Program (2009-0087691) of NRF/MEST, and Global Research Lab (NRF-2013K1A1A2035662). The work at Min group (J.S., J.Y.K., S.L. and B.M.) was supported by the National Research Foundation of Korea (NRF) grant funded by the Korea government (MEST) (NRF-2013-065650, 2013-050154) and by the World Class Institute (WCI) Program of the National Research Foundation of Korea (NRF) funded by the Korea government (WCI 2011-001), and in part by the Center for Integrated Smart Sensors funded by the Ministry of Science, ICT & Future Planning as Global Frontier Project (CISS-2013-072208).